ARTICLES SCIENCE CHINA Materials

mater.scichina.com link.springer.com

Published online 6 February 2017 | doi: 10.1007/s40843-016-9002-y
Sci China Mater 2017, 60(4): 304–314

Fast synthesis of uniform mesoporous titania submicrospheres with high tap densities for high-volumetric performance Li-ion batteries

Kunlei Zhu[1,2], Yinghui Sun[3], Rongming Wang[3], Zhongqiang Shan[1*] and Kai Liu[2*]

ABSTRACT **High-tap density electrode materials are greatly desired for Li-ion batteries with high volumetric capacities to fulfill the growing demands of electric vehicles and portable smart devices. TiO_2, which is one of the most attractive anode materials, is limited in their application for Li-ion batteries because of its low tap density (usually <1 g cm^{-3}) and volumetric capacity. Herein, we report uniform mesoporous TiO_2 submicrospheres with a tap density as high as 1.62 g cm^{-3} as a promising anode material. Even with a high mass loading of 24 mg cm^{-2}, the TiO_2 submicrospheres have impressive volumetric capacities that are more than double those of their counterparts. Moreover, they can be synthesized with ~100% yield and within a reaction time of ~6 h by optimizing the experimental conditions and formation mechanism, exhibiting potential for large-scale production for industrial applications. Other mesoporous anode materials, i.e., high-tap density mesoporous $Li_4Ti_5O_{12}$ submicrospheres, are fabricated using the generalized method. We believe that our work provides a significant reference for the industrial production of mesoporous materials for Li-ion batteries with a high volumetric performance.**

Keywords: fast synthesis, Li-ion batteries, mesoporous materials, TiO_2, volumetric performance

INTRODUCTION

Volumetric performance is of vital importance for electrochemical energy-storage devices, considering the energy output in a limited space for electric vehicles and portable smart devices [1–3]. One strategy for improving the volumetric performance is to promote the volumetric capacity of the electrode materials [4,5]. Although the nanomaterials used as electrode materials show an impressive gravimetric capacity, they usually have an extremely low tap density [6], inevitably leading to an unsatisfactory volumetric capacity. Thus, electrode materials with a high tap density are needed to improve the volumetric performance of energy-storage devices. Mesoporous materials with pore sizes of 2–50 nm are ideal candidates [4]. They have not only abundant pores, facilitating the entry of electrolytes and the transport of Li ions, but also a high tap density, which improves the volumetric performance.

As one of the most attractive candidates for anode materials of Li-ion batteries, TiO_2 has drawn increasing interest [4,7–11]. It has several remarkable characteristics, including its low cost, environmental non-toxicity, a high operation voltage (suppressing the formation of solid-electrolyte interphase layers and Li dendrites), a small volume change, and a robust structure. However, the tap density of TiO_2 materials is low. For example, Yu *et al.* [12] reported rutile TiO_2 submicroboxes with superior Li-storage performance but a TiO_2 tap density of only 0.44 g cm^{-3}. The tap density of TiO_2-(B) was improved by using large starting materials [13], but the value was only 0.67 g cm^{-3}. Saravanan *et al.* [4] reported mesoporous TiO_2 with impressive capacities nearly five times better than those of commercially available TiO_2 nanopowders. However, the tap density of the mesoporous TiO_2 is only 0.714 g cm^{-3}, which limits its volumetric capacity. Thus, the mesoporous TiO_2 with a high tap density is highly desirable for improving the volumetric capacity of Li-ion batteries with high mass loading.

The mesoporous TiO_2 submicrospheres composed of

[1] School of Chemical Engineering and Technology, Tianjin University, Tianjin 300072, China
[2] State Key Laboratory of New Ceramics and Fine Processing, School of Materials Science and Engineering, Tsinghua University, Beijing 100084, China
[3] Beijing Key Laboratory for Magneto-Photoelectrical Composite and Interface Science, School of Mathematics and Physics, University of Science and Technology Beijing, Beijing 100083, China
[*] Corresponding authors (emails: shanzq@tju.edu.cn (Shan Z); liuk@tsinghua.edu.cn (Liu K))

densely packed nanocrystals are an excellent choice for high-tap density TiO_2 materials [14]. In addition to the aforementioned advantages, mesoporous TiO_2 submicrospheres have abundant pores, densely packed nanocrystals, a relatively large size, and a spherical morphology, granting them unique traits, including adequate access for electrolyte entry, a high tap density, the absence of aggregation, and the formation of a compact electrode layer [15–17]. Soft-templating method is one of the most common methods for the synthesis of high-quality mesoporous TiO_2 spheres. However, the synthesis is usually complex [18–20], tedious [21–23], and time-consuming (see Table S1) [24,25]. For example, the fabrication of uniform mesoporous TiO_2 beads involves a two-step method: an 18 h sol-gel process followed by 16 h of solvothermal treatment in the presence of *n*-hexadecylamine (HDA) as a structure-directing agent (SDA) [17,21]. The mesoporous beads were obtained via solvothermal treatment for 24 h using a PVC-g-POEM graft copolymer as an SDA [23]. There are reports of the fast synthesis of mesoporous TiO_2 within several hours, but the products are aggregated [26–28], amorphous [29], uneven [30] or in bulk [31,32]. Although mesoporous hollow TiO_2 spheres have been intensively investigated [11,33,34], their low density/tap density can lead to a low volumetric performance. In addition, hierarchical mesoporous TiO_2 nanowire bundles (HM-TiO_2-NB) with a tap density as high as 1.63 g cm^{-3} were synthesized by using the triblock copolymer P123 as a soft template [35]. However, their fabrication process took over 48 h (Table S1), inevitably increasing the cost of large-scale production. Thus, the simple and fast synthesis of uniform mesoporous TiO_2 submicrospheres (UMTSs) with a high tap density remains very challenging.

Herein, we report UMTSs as a promising anode material with a tap density as high as 1.62 g cm^{-3}. Even with a high mass loading of 24 mg cm^{-2}, the UMTSs have a volumetric capacity of ~70 mA h cm^{-3} after 50 cycles at 1 C (1 C = 170 mA g^{-1}), which is superior to the performance of their counterparts. Moreover, they were fabricated with a yield of ~100% and within a reaction time of 6 h, exhibiting potential for large-scale production for industrial applications. Other mesoporous anode materials, i.e., high-tap density mesoporous $Li_4Ti_5O_{12}$ submicrospheres, were synthesized using the generalized method. This work provides a significant reference for the industrial production of mesoporous materials in Li-ion batteries with a high volumetric performance.

EXPERIMENTAL SECTION

Chemicals

HDA (90%) and titanium isopropoxide (TTIP, 98%) were purchased from ACROS. Absolute ethanol (>99.7%), concentrated ammonia water (~25 wt.%), and glacial acetic acid were obtained from Tianjin Guangfu Fine Chemical Research Institute. Cetyl trimethyl ammonium bromide (99%) and hydrochloric acid were provided by Tianjin Kemiou Chemical Reagent Co., Ltd. Sodium dodecyl benzene sulfonate (95%), and lithium hydroxide monohydrate ($LiOH{\cdot}H_2O$, 98%) were purchased from Aladdin.

Fast synthesis of UMTSs

Instead of the previously reported two-step method combining sol-gel and solvothermal processes [21], we adopted a fast and facile solvothermal method using HDA as an SDA, as follows. First, 1.5 g of HDA was dissolved in 150 mL of absolute ethanol, followed by the addition of 1.8 mL of concentrated ammonia water. Then, 3.0 mL of TTIP was added to the aforementioned mixture under vigorous stirring at 30°C, yielding a white precursor suspension. The precursor suspension was directly transferred into a 200 mL Teflon-lined stainless-steel autoclave without aging and treated with a solvothermal process at 200°C for 4 h. After being centrifuged and washed with ethanol three times, the air-dried white powder (intermediate TiO_2) was prepared. The intermediate TiO_2 was calcined at 500°C for 2 h in the ambient air to remove any organic species, and the final product—UMTSs—was obtained. The total reaction time was only 6 h (including the solvothermal and calcination time). Synthesis of one batch produced ~0.79 g UMTSs. The yield of UMTSs was calculated to be ~100% using the following equation:

$$mM_2 / M_1 \rho V p \times 100\%, \quad (1)$$

where m is the mass of UMTSs; M_1 (79.87 g moL^{-1}) is the molar mass of TiO_2; and M_2 (284.22 g moL^{-1}), ρ (0.96 g mL^{-1}), V (3 mL), and p (98%) are the molar mass, density, volume, and purity of TTIP, respectively.

Fast synthesis of uniform mesoporous $Li_4Ti_5O_{12}$ submicrospheres

In a typical synthesis procedure, 1.0 g of HDA was dissolved in 100 mL of absolute ethanol, followed by the addition of 1.2 mL of concentrated ammonia water. Next, 2.0 mL of TTIP was added to the aforementioned mixture under vigorous stirring at 30°C. Then, 50 mL of absolute ethanol

(containing $LiOH{\cdot}H_2O$, Li/Ti = 1/1) was poured into the reaction solution. The resulting solution was directly transferred into a 200 mL Teflon-lined stainless-steel autoclave without aging and kept at 200°C for 12 h. After centrifugation and ethanol washing, the intermediate product was calcined at 500°C for 2 h in the ambient air to remove any organic species, yielding mesoporous $Li_4Ti_5O_{12}$ submicrospheres.

Material characterizations and measurements

X-ray diffraction (XRD) patterns were obtained using a Rigaku D/max 2500 PC diffractometer (Japan). Raman spectra were obtained using a DXR Microscope (USA) under 632.8-nm excitation. Scanning electron microscopy (SEM) and energy-dispersive X-ray spectroscopy (EDS) were performed using a Hitachi S-4800 microscope (Japan, 15 kV) equipped with a Thermo Scientific energy-dispersion X-ray fluorescence analyzer. For the EDS analysis, the samples were dispersed in ethanol and dropped on a Cu substrate to avoid C signals from the conductive adhesive used to fix the samples. Transmission electron microscopy (TEM) was performed using a JEOL JEM-2100F microscope (Japan) operated at 200 kV. Scanning TEM high-angle annular dark-field (STEM-HAADF) imaging and electron energy-loss spectroscopy (EELS) were performed using a FEI Tecnai G2 F20. The N_2 adsorption/desorption isotherms were obtained using a Quantachrome NOVA instrument and a micromeritics surface area and porosity analyzer (ASAP 2020 HD88). The pore-size distribution curve was calculated using Barrett-Joyner-Halenda (BJH) pore-size analysis of the N_2 gas desorption curve.

The electrochemical performance was investigated at room temperature using 2032 coin cells. The anodes were prepared by mixing the active materials—acetylene black and polytetrafluoroethylene (PTFE)—at a weight ratio of 70:20:10. We pressed a mixture containing 27.1 mg of TiO_2, 5.8 mg of acetylene black, and 9.7 mg of PTFE (60% solution) into circular tablets 12 mm in diameter using a homemade device with a constant pressure. The film thickness of the uniform mesoporous TiO_2 with 24 mg cm^{-2} mass loading was ~0.5 mm, whereas the value for commercial TiO_2 is ~1 mm. Li was employed as both the counter electrode and the reference electrode. The gravimetric capacity and volumetric capacity were calculated according to the mass of TiO_2 and the volume of the electrodes, respectively. For the electrolyte, 1 mol L^{-1} $LiPF_6$ dissolved in a mixture of ethylene carbonate, diethyl carbonate, and dimethyl carbonate (1:1:1 in volume) was used. Galvanostatic charge/discharge tests were performed using a LAND CT2001A battery-test system. Cyclic voltammetry (CV) (0.1 mV s^{-1}) was performed using an LK 3200 electrochemical workstation. The voltage windows were 1–3 V (*vs.* Li^+(1 mol L^{-1})/Li) for TiO_2. Electrochemical impedance spectroscopy (EIS) was performed using an electrochemical station (IM6e, Zahner, Germany) with an applied perturbation of 5 mV.

RESULTS AND DISCUSSION

Fast synthesis of UMTSs with high tap density

Fig. 1 shows the synthesis process for the UMTSs. After the addition of TTIP into the ethanol solution containing HDA and concentrated ammonia water, smooth precursor spheres were obtained. These amorphous inorganic-organic composites consisting of $Ti(OCH(CH_3)_2)_{4-x}(OH)_x$-HDA (TOH) hybrid species were formed via hydrogen-bonding interactions between the hydrolyzed products of $Ti(OCH(CH_3)_2)_{4-x}(OH)_x$ species and amino groups of HDA (Fig. S1) [21]. The precursor solutions were directly transferred into a Teflon-lined stainless-steel autoclave without aging for the fast synthesis. The intermediate TiO_2 samples were fabricated within 4 h, which was far shorter than the combined 18 h sol-gel and 16 h solvothermal processes reported in the literature [21]. During the solvothermal treatment, some HDA species escaped from the hybrid composites, leaving vacancies within the intermediate, well-crystallographic, and robust TiO_2 because of the destruction of the hydrogen-bonding interactions of HDA and $Ti(OCH(CH_3)_2)_{4-x}(OH)_x$, which was caused by the condensation of –OH species (see the Supplementary information for detailed discussions on the mechanism). After 2 h of calcination in the ambient air, the spherical structure was maintained, and the vacancies were connected together, leading to the formation of UMTSs composed of nanocrystals with pores (Fig. 2). The reaction was controlled so that the pores were well maintained, the nanocrystals were tightly packed, and the spheres were not merged together, ensuring the porosity, high tap density, and uniformity of the UMTSs. In addition, a series of systematic experiments (Figs S1–S10) indicated that the solvothermal time could be shortened by elevating the solvothermal temperature and the specific surface area increased at higher temperatures (Fig. S11), which implies that UMTSs are fabricated more quickly if the solvothermal temperature is increased appropriately.

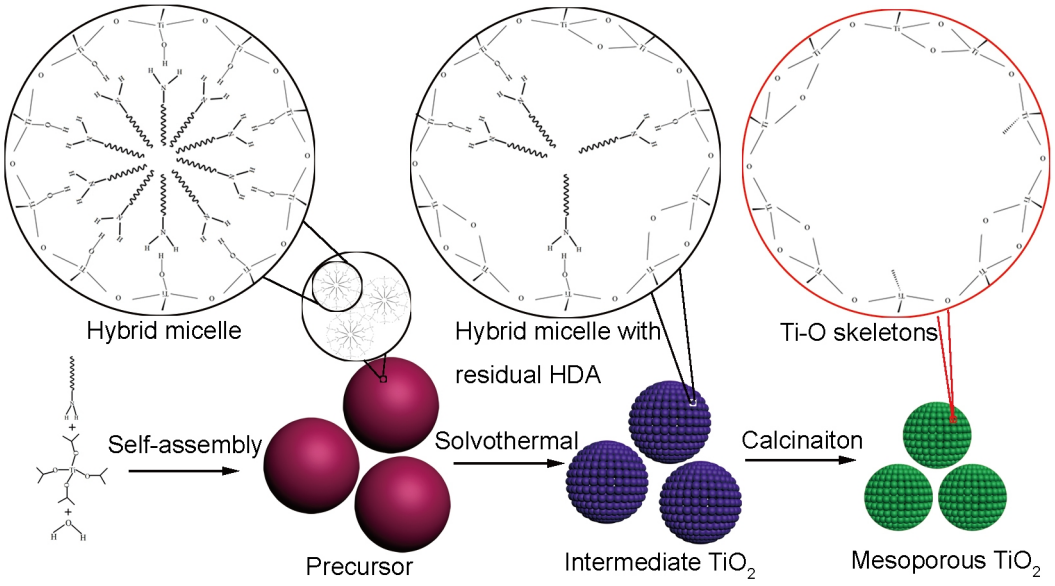

Figure 1 Schematic of the synthesis of the UMTSs.

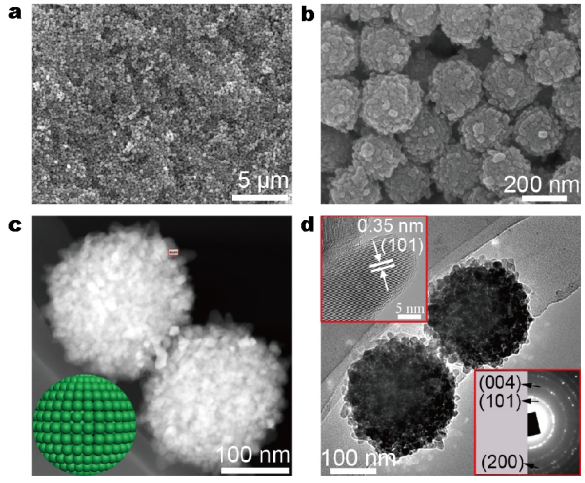

Figure 2 SEM (a, b), STEM (c), and TEM images (d) of anatase UMTSs. The upper and lower insets in d show an HRTEM image and an SAED pattern, respectively.

The SEM image (Fig. 2a) shows the morphology of the UMTSs. The spheres were uniform and ~240 nm in size. Their sizes were controlled between ~200 and ~330 nm by changing the amount of concentrated ammonia water (Fig. S13). They have a rough surface and are composed of 6–25 nm (13.8 nm in mean) nanocrystals, as revealed by the high-resolution SEM image shown in Fig. 2b. These nanocrystals are loosely connected, indicating that pores form among them. However, the pores are disordered, as revealed by the low-angle XRD pattern shown in Fig. S14. Both the EELS (Fig. S15) for the red region in Fig. 2c and the EDS spectrum (Fig. S16) exhibit only peaks of Ti and O, suggesting that the samples are pure TiO_2 and that the organic components are completely removed.

The STEM-HAADF image shown in Fig. 2c clearly shows the TiO_2 spheres consisting of 7–24 nm (13.2 nm in mean) nanocrystals, which is consistent with the SEM images. The TEM image shown in Fig. 2d confirms that the TiO_2 spheres consist of nanocrystals and contain plenty of pores, as indicated by the scattered white dots. The high-resolution TEM (HRTEM) image (upper inset in Fig. 2d) reveals well-defined crystalline lattices with a *d*-spacing of 0.35 nm, which are assigned to the (101) planes of anatase TiO_2. The selected-area electron diffraction (SAED) pattern (Fig. 2d, lower inset) acquired for a single sphere exhibits a series of diffraction rings, indicating that the TiO_2 spheres are polycrystalline.

The XRD pattern confirms the anatase phase (JCPDS card No. 21-1272; $a_0 = b_0 = 0.37852$ nm, $c_0 = 0.95139$ nm; space group *I*41/*amd*) of the UMTSs, as shown in Fig. 3a. The crystal size of the basic nanoparticles is ~15.2 nm, as calculated using the full width at half maximum of the (101) peak via the Scherrer equation. This agrees well with the aforementioned observations. The Raman spectrum (Fig. 3b) confirms that the calcined samples are pure anatase TiO_2 without any residual organic species (e.g., C).

The N_2 adsorption-desorption isotherms (Fig. 3c) reveal a type-IV isotherm with a type-H3 hysteresis loop at the

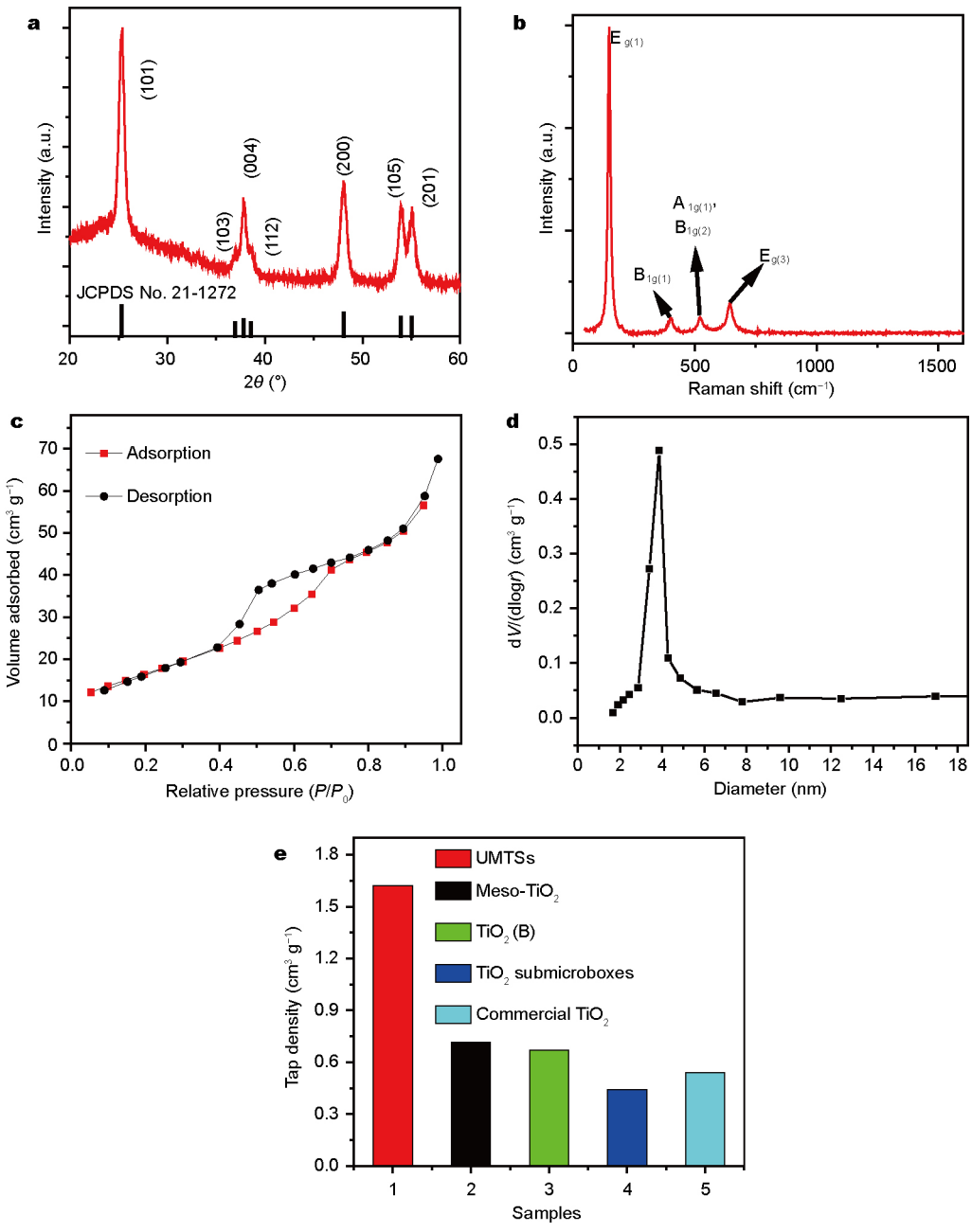

Figure 3 XRD pattern (a), Raman spectrum (b), N_2 adsorption/desorption isotherm (c), and pore-size distribution curve (d) of uniform TiO_2 spheres. Chart of the tap density of the UMTSs, meso-TiO_2 [4], TiO_2(B) [13], TiO_2 submicroboxes [12], and commercial TiO_2 (e).

relative pressures of P/P_0 = 0.4–0.75 for the UMTSs. The curves are typical for mesoporous solids [11,21]. The specific surface area of the TiO_2 spheres was estimated to be 60.9 $m^2 g^{-1}$ using the multi-point Brunauer–Emmett–Teller method. The curve shown in Fig. 3d indicates a narrow pore-size distribution centered at ~3.9 nm, suggesting that uniform mesopores exist among the nanocrystals of the spheres.

The tap density of the UMTSs is as high as 1.62 g cm^{-3}, which is far higher than that of meso-TiO_2 (0.714 g cm^{-3}) [4], TiO_2 submicroboxes (0.44 g cm^{-3}) [12], TiO_2(B) (0.67 g cm^{-3}) [13], and commercial TiO_2 (0.54 g cm^{-3}) (Fig. 3e). Efficient synthesis of ~0.79 g of UMTSs with a yield of ~100% (ratio of the mass of UMTSs to the theoretical mass of TiO_2) is achieved in one batch within a reaction time of 6 h, suggesting fast and high-yield production. These

UMTSs with high tap densities are favorable for the fabrication of compact electrodes, which are expected to improve the volumetric capacities of Li-ion batteries. The facile, fast, and high-yield synthesis of the materials exhibits great potential for the large-scale and cost-effective production of high-performance electrodes for Li-ion batteries.

Generalization of the fast synthesis to fabricate mesoporous $Li_4Ti_5O_{12}$ submicrospheres

Interestingly, our synthesis method for UMTSs was generalized to fabricate other mesoporous anode materials, i.e., uniform mesoporous $Li_4Ti_5O_{12}$ submicrospheres. To synthesize the mesoporous $Li_4Ti_5O_{12}$ spheres, TTIP was added to an ethanol solution containing HDA and concentrated ammonia water, followed by the introduction of LiOH. The resulting mixture was subjected to solvothermal treatment at 200°C for 12 h, followed by 2 h of calcination. As shown in Fig. 4a, the uniform spheres are generally ~240 nm in size and are composed of 10–20 nm nanocrystals. TEM and STEM images (Fig. 4b, c) confirm that the spheres comprise numerous fluffy nanocrystals. Abundant pores are present among these nanocrystals (Fig. 4a–c). According

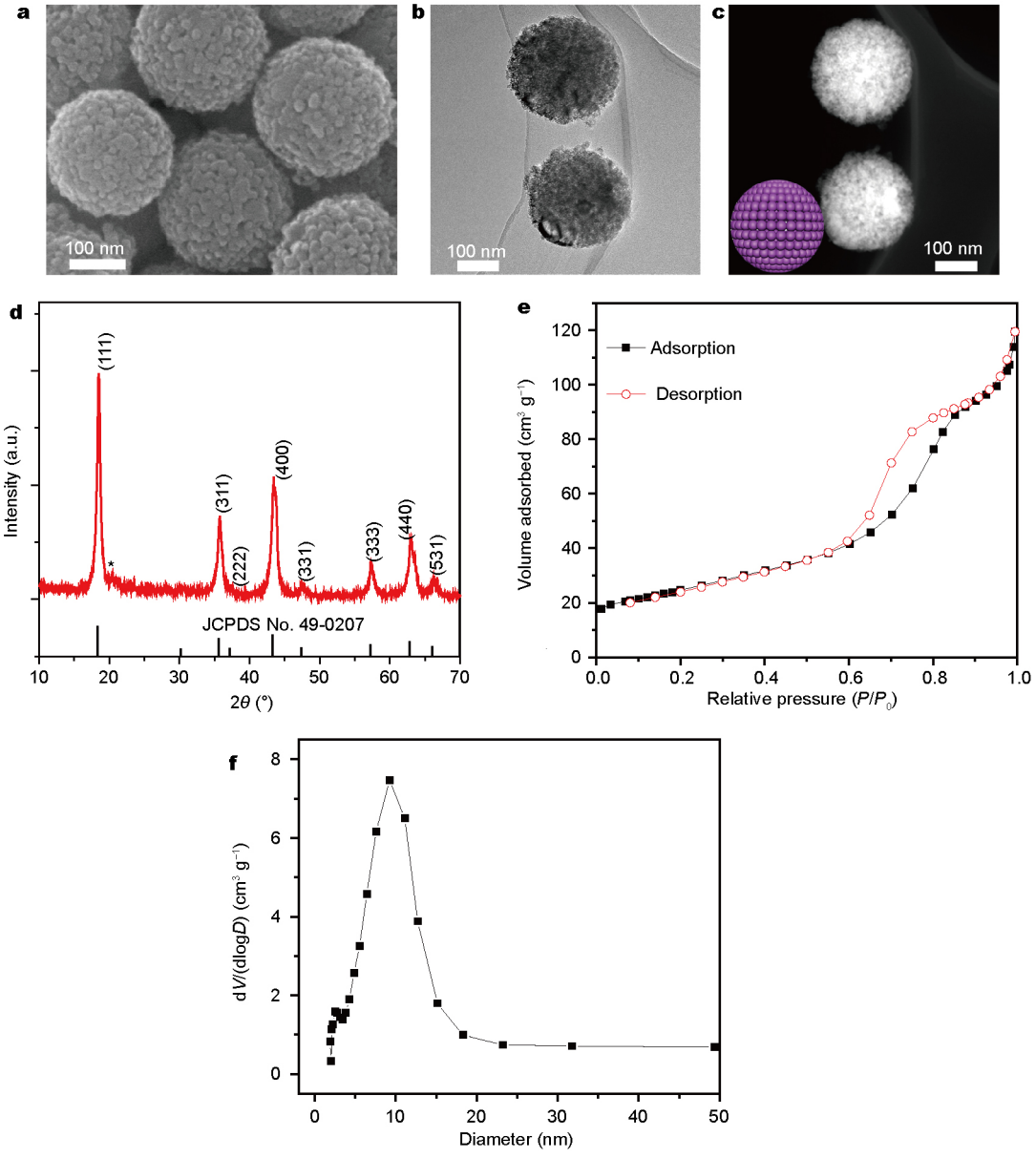

Figure 4 Uniform mesoporous $Li_4Ti_5O_{12}$ submicrospheres: SEM (a), TEM (b), and STEM (c) images; XRD pattern (d); N_2 adsorption/desorption isotherm (e); and pore-size distribution curve (f). The peak marked by the asterisk at ~20.4° is indexed to Li_2TiO_3.

to the XRD pattern (Fig. 4d), the spheres are indexed to spinel $Li_4Ti_5O_{12}$ [36]. The N_2 adsorption/desorption isotherm was measured to check their porosity (Fig. 4e), and their specific surface area was calculated to be ~86.7 $m^2 g^{-1}$. The pore-size distribution curve of the $Li_4Ti_5O_{12}$ spheres is centered at ~7.3 nm (Fig. 4f), and the pores are disordered (Fig. S14). Thus, the synthesis of sub-microsize, uniform, and mesoporous $Li_4Ti_5O_{12}$ spheres is achieved. These submicrospheres have a tap density as high as 1.33 g cm^{-3}, which is higher than that of commercial $Li_4Ti_5O_{12}$ materials (~1.0 g cm^{-3}), indicating their potential for industrial applications.

Electrochemical performance of UMTSs

Fig. 5a shows the galvanostatic charge/discharge curves of the UMTSs for the first three cycles over a voltage range of 1–3 V at 0.1 C. The galvanostatic discharge process can be divided into three stages. The first stage shows a sharp drop from the open-circuit voltage to ~1.75 V, corresponding to the formation of a solid solution domain of tetragonal

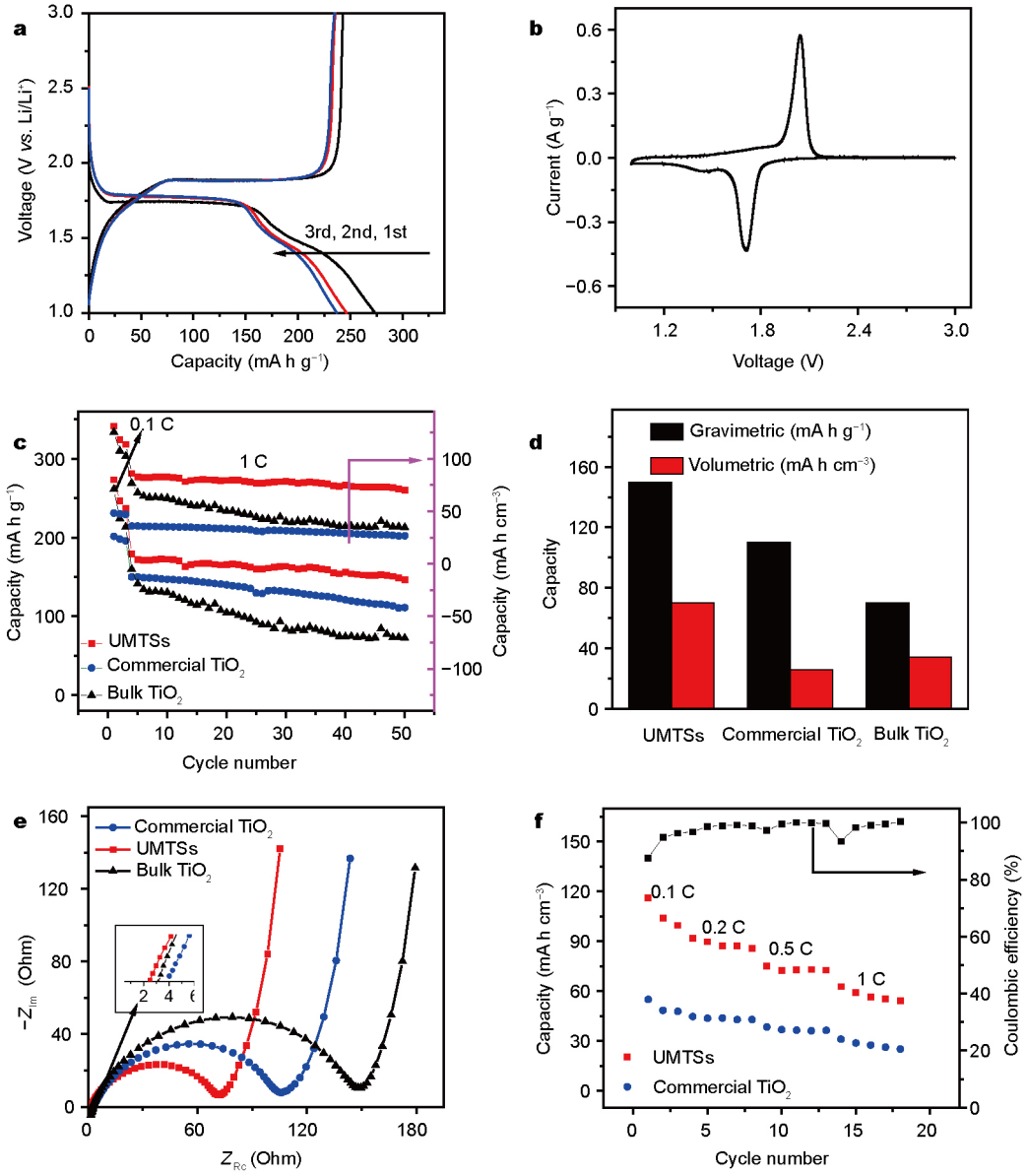

Figure 5 Galvanostatic charge/discharge curves for the first three cycles at 0.1 C (a) and CV curve obtained at a scan rate of 0.1 mV s^{-1} for the UMTSs. The cycle-performance curves at 1 C (c), a performance-comparison chart (d), and the EIS (e) of the three samples. Volumetric rate capability curves (e) of the UMTSs and commercial TiO_2. The mass loading of all the electrodes was 24 mg cm^{-2}.

anatase TiO_2 ($I4_1/amd$) and Li-poor tetragonal Li_xTiO_2 ($I4_1/amd$), with a small fraction of the Li intercalating into the bulk TiO_2 [16,17]. The second stage exhibits an obvious discharge plateau at ~1.75 V, resulting from the phase-coexisting domain of the Li-poor tetragonal Li_xTiO_2 and the newly formed Li-rich orthorhombic $Li_{0.5}TiO_2$ (*Imma*) with further Li insertion [8,11,16]. The last stage—below ~1.75 V—involves the further storage of Li ions on the surface/interface of TiO_2 [17,37,38], which leads to an inconspicuous peak at ~1.5 V. The first discharge capacity is 273.4 mA h g^{-1}, and the subsequent charge capacity is 243 mA h g^{-1}, leading to a Coulombic efficiency of 88.9% for the first cycle, which is probably due to the trapping of some Li ions within UMTSs. However, the efficiencies increase to 95.6% and 99.1% in the second and third cycles, respectively.

Fig. 5b shows the CV of UMTSs obtained at a scan rate of 0.1 mV s^{-1}. The pair of cathodic/anodic peaks at ~1.71/2.01 V corresponds to the insertion/extraction of Li^+ ions in/out of the UMTSs. The peak at ~1.71 V is characteristic of the biphasic transition from tetragonal anatase ($I4_1/amd$) to orthorhombic $Li_{0.5}TiO_2$ (*Imma*) and is consistent with the galvanostatic curve. In addition to the two aforementioned typical peaks, there is another pair of peaks at ~1.80/1.45 V, probably arising from the Li storage on the surface/interface of mesoporous TiO_2, which has been previously reported [17,37,38].

The cycle performance is shown in Fig. 5c. The cells were activated for the first three cycles at 0.1 C. After 50 cycles at 1 C, the UMTSs still have a discharge capacity of ~150 mA h g^{-1}, even with a mass loading of 24 mg cm^{-2}. The Coulombic efficiency of each cycle almost reaches 100% (Fig. S17). In addition, the capacities of the mesoporous TiO_2 spheres are maintained at ~170 mA h g^{-1}, independent of the mass loading of active materials ≤ 24 mg cm^{-2} (Fig. S18). Even if the mass loading reaches 44 mg cm^{-2}, a discharge capacity as high as ~150 mA h g^{-1} is obtained. In comparison, commercially available anatase TiO_2 (25 nm in size) calcined at 500°C for 2 h before use and bulk TiO_2 comprising nanoparticles fabricated without HDA (Fig. S11) only provide discharge capacities of ~110 and ~70 mA h g^{-1}, respectively, after 50 cycles. Because of their high tap density, the mesoporous TiO_2 spheres have a far higher volumetric storage capacity (~70 mA h cm^{-3}) after 50 cycles than their counterparts (~26 and ~34 mA h cm^{-3} for commercial TiO_2 and bulk TiO_2, respectively). A comparison is shown in Fig. 5d. Notably, the volumetric capacity of the UMTSs is more than double those of commercial and bulk TiO_2.

The EIS (Fig. 5e) of the three materials all exhibit a semicircle and a linear Warburg region spanning the high-, medium-, and low-frequency areas. The high-frequency region is associated with the internal resistance, including the resistance of the separator, the electrode/electrolyte interface, and the electrical contact. Among the three materials compared in the inset of Fig. 5e, the UMTSs have the smallest internal resistance, indicating the effective electron transport. The medium region is related to the charge-transfer resistance in the interfacial transfer of Li ions. The semicircle for the UMTSs has the smallest diameter, indicating the smallest charge-transfer resistance. Thus, the mesoporous TiO_2 spheres with the enhanced reaction kinetics promote the transfer and exchange of electrons, Li ions, and electrolytes, improving the electrochemical performance.

The rate capacity is an important parameter for Li-ion batteries. The values for the UMTSs and commercial TiO_2 are presented in Fig. 5f and Fig. S19. Although their gravimetric capacities are comparable (Fig. S19), the volumetric capacities of the UMTSs are double those of commercial TiO_2 (Fig. 5f). Because of their high tap density, the UMTSs have volumetric capacities of ~105, ~90, ~75, and ~60 mA h cm^{-3} at 0.1, 0.2, 0.5 and 1 C, respectively, which are substantially higher than the corresponding values of the commercial TiO_2 (~50, ~42, ~36, and ~26 mA h cm^{-3}, respectively). In addition, the Coulombic efficiency of the UMRSs is almost 100% in each cycle at various currents (Fig. 5f).

To clearly explain the good performance of the UMTSs, a schematic is presented in Fig. 6. The mechanism can be explained as follows. 1) The UMTSs have a large specific area, providing abundant Li-insertion sites. 2) The mesopores within the UMTSs facilitate the entry of Li^+ ions and the electrolyte, which maximizes the contact between the TiO_2 nanocrystals and Li^+ ions, reducing the diffusion distance of the Li^+ ions. 3) The UMTSs with a sub-microsize diameter are free of aggregation, which usually occurs for nanomaterials. This is beneficial for the uniform coating of the conductive agent onto the spheres during the electrode fabrication, which is believed to improve the transmission of electrons. 4) The spherical mesoporous TiO_2 has better particle mobility, leading to the formation of a more compact electrode layer [15,16]. More importantly, the UMTSs have a very high tap density and are thus capable of forming compact electrodes and yielding a high volumetric performance. They are expected to be promising materials in other fields, such as catalysis, photovoltaics, drug delivery, and sensors [39–41].

The electrochemical performance of the uniform meso-

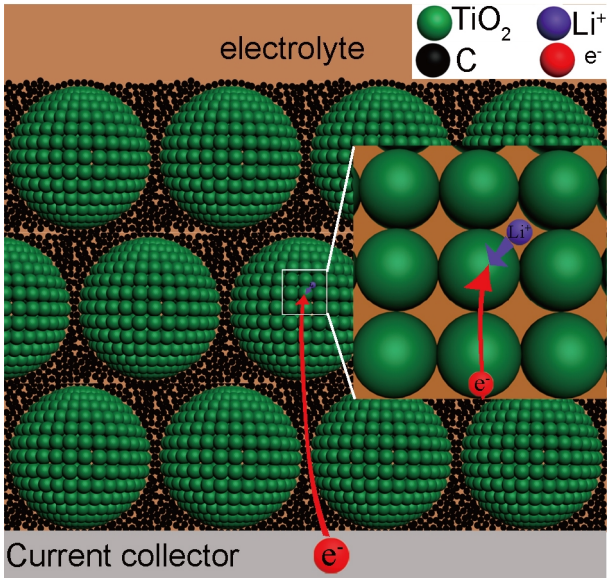

Figure 6 Schematic of the transport path of Li ions and electrons within the UMTS-based electrodes.

porous $Li_4Ti_5O_{12}$ spheres is shown in Fig. S20. Their performance is comparable to that of mesoporous $Li_4Ti_5O_{12}$ prepared by a two-step method. For example, $Li_4Ti_5O_{12}$ prepared by a two-step method had a discharge capacity of ~110 mA h g^{-1} at 10 C (1 C = 175 mA g^{-1}) after 100 cycles [36], and our mesoporous $Li_4Ti_5O_{12}$ spheres have a corresponding value of ~120 mA h g^{-1}. Thus, the uniform mesoporous $Li_4Ti_5O_{12}$ spheres with a high tap density demonstrate good electrochemical performance and potential for industrial applications.

CONCLUSION

We prepared TiO_2 UMTSs with a high tap density and ~100% yield via a fast solvothermal method. These UMTSs were demonstrated to be potential candidates for high-volumetric performance Li-ion batteries. Uniform mesoporous $Li_4Ti_5O_{12}$ submicrospheres with a high tap density were fabricated using a similar method. Our results can be applied for improving the volumetric performance of Li-ion batteries and realizing the large-scale production of mesoporous materials.

Received 19 December 2016; accepted 18 January 2017; published online 6 February 2017

1 Gogotsi Y, Simon P. True performance metrics in electrochemical energy storage. Science, 2011, 334: 917–918
2 Ghidiu M, Lukatskaya MR, Zhao MQ, *et al.* Conductive two-dimensional titanium carbide 'clay' with high volumetric capacitance. Nature, 2014, 516: 78–81
3 Zhang C, Yang QH. Packing sulfur into carbon framework for high volumetric performance lithium-sulfur batteries. Sci China Mater, 2015, 58: 349–354
4 Saravanan K, Ananthanarayanan K, Balaya P. Mesoporous TiO_2 with high packing density for superior lithium storage. Energy Environ Sci, 2010, 3: 939–948
5 Liang J, Yu XY, Zhou H, *et al.* Bowl-like SnO_2@carbon hollow particles as an advanced anode material for lithium-ion batteries. Angew Chem Int Ed, 2014, 53: 12803–12807
6 Wagemaker M, Mulder FM. Properties and promises of nanosized insertion materials for Li-ion batteries. Acc Chem Res, 2013, 46: 1206–1215
7 Li W, Wu Z, Wang J, *et al.* A perspective on mesoporous TiO_2 materials. Chem Mater, 2014, 26: 287–298
8 Qiu B, Xing M, Zhang J. Mesoporous TiO_2 nanocrystals grown *in situ* on graphene aerogels for high photocatalysis and lithium-ion batteries. J Am Chem Soc, 2014, 136: 5852–5855
9 Liu Y, Che R, Chen G, *et al.* Radially oriented mesoporous TiO_2 microspheres with single-crystal-like anatase walls for high-efficiency optoelectronic devices. Sci Adv, 2015, 1: e1500166
10 Liu Y, Elzatahry AA, Luo W, *et al.* Surfactant-templating strategy for ultrathin mesoporous TiO_2 coating on flexible graphitized carbon supports for high-performance lithium-ion battery. Nano Energy, 2016, 25: 80–90
11 Guan BY, Yu L, Li J, *et al.* A universal cooperative assembly-directed method for coating of mesoporous TiO_2 nanoshells with enhanced lithium storage properties. Sci Adv, 2016, 2: e1501554
12 Yu XY, Wu HB, Yu L, *et al.* Rutile TiO_2 submicroboxes with superior lithium storage properties. Angew Chem Int Ed, 2015, 54: 4001–4004
13 Saito M, Nakano Y, Takagi M, *et al.* Improvement of tap density of TiO_2(B) powder as high potential negative electrode for lithium ion batteries. J Power Sources, 2013, 244: 50–55
14 Chen D, Caruso RA. Recent progress in the synthesis of spherical titania nanostructures and their applications. Adv Funct Mater, 2013, 23: 1356–1374
15 Liu H, Bi Z, Sun XG, *et al.* Mesoporous TiO_2-B microspheres with superior rate performance for lithium ion batteries. Adv Mater, 2011, 23: 3450–3454
16 Trang NTH, Ali Z, Kang DJ. Mesoporous TiO_2 spheres interconnected by multiwalled carbon nanotubes as an anode for high-performance lithium ion batteries. ACS Appl Mater Interfaces, 2015, 7: 3676–3683
17 Zhu K, Tian J, Liu Y, *et al.* Submicron-sized mesoporous anatase TiO_2 beads with a high specific surface synthesized by controlling reaction conditions for high-performance Li-batteries. RSC Adv, 2013, 3: 13149–13155
18 Zhao T, Luo W, Deng Y, *et al.* Monodisperse mesoporous TiO_2 microspheres for dye sensitized solar cells. Nano Energy, 2016, 26: 16–25
19 Zhang Y, Shi Y, Liou YH, *et al.* High performance separation of aerosol sprayed mesoporous TiO_2 sub-microspheres from aggregates via density gradient centrifugation. J Mater Chem, 2010, 20: 4162–4167
20 Hong MP, Kim JY, Vemula K, *et al.* Synthesis of monodisperse mesoporous TiO_2 spheres with tunable sizes between 0.6 and 3.1 μm and effects of reaction temperature, Ti source purity, and type of alkylamine on size and monodispersity. Chem Commun, 2012, 48: 4250–4252
21 Chen D, Cao L, Huang F, *et al.* Synthesis of monodisperse mesoporous titania beads with controllable diameter, high surface areas, and variable pore diameters (14–23 nm). J Am Chem Soc, 2010, 132: 4438–4444

22 Yan K, Qiu Y, Chen W, *et al.* A double layered photoanode made of highly crystalline TiO_2 nanooctahedra and agglutinated mesoporous TiO_2 microspheres for high efficiency dye sensitized solar cells. Energy Environ Sci, 2011, 4: 2168–2176
23 Roh DK, Seo JA, Chi WS, *et al.* Facile synthesis of size-tunable mesoporous anatase TiO_2 beads using a graft copolymer for quasi-solid and all-solid dye-sensitized solar cells. J Mater Chem, 2012, 22: 11079–11085
24 Wang L, Tomura S, Maeda M, *et al.* Synthesis of mesoporous TiO_2 spheres under static condition. Chem Lett, 2000, 29: 1414–1415
25 Duan Y, Fu N, Fang Y, *et al.* Synthesis and formation mechanism of mesoporous TiO_2 microspheres for scattering layer in dye-sensitized solar cells. Electrochim Acta, 2013, 113: 109–116
26 Wang Y, Tang X, Yin L, *et al.* Sonochemical synthesis of mesoporous titanium oxide with wormhole-like framework structures. Adv Mater, 2000, 12: 1183–1186
27 Zhang L, Yu JC. A sonochemical approach to hierarchical porous titania spheres with enhanced photocatalytic activity. Chem Commun, 2003, 9: 2078
28 Wang HE, Jin J, Cai Y, *et al.* Facile and fast synthesis of porous TiO_2 spheres for use in lithium ion batteries. J Colloid Interface Sci, 2014, 417: 144–151
29 Widoniak J, Eiden-Assmann S, Maret G. Synthesis and characterisation of porous and non-porous monodisperse TiO_2 and ZrO_2 particles. Colloids Surfaces A-Physicochem Eng Aspects, 2005, 270-271: 329–334
30 Tsung CK, Fan J, Zheng N, *et al.* A general route to diverse mesoporous metal oxide submicrospheres with highly crystalline frameworks. Angew Chem Int Ed, 2008, 47: 8682–8686
31 Das SK, Darmakolla S, Bhattacharyya AJ. High lithium storage in micrometre sized mesoporous spherical self-assembly of anatase titania nanospheres and carbon. J Mater Chem, 2010, 20: 1600
32 Tong H, Enomoto N, Inada M, *et al.* Synthesis of mesoporous TiO_2 spheres and aggregates by sol-gel method for dye-sensitized solar cells. Mater Lett, 2015, 141: 259–262
33 Liu H, Li W, Shen D, *et al.* Graphitic carbon conformal coating of mesoporous TiO_2 hollow spheres for high-performance lithium ion battery anodes. J Am Chem Soc, 2015, 137: 13161–13166
34 Liu H, Ma H, Joo J, *et al.* Contribution of multiple reflections to light utilization efficiency of submicron hollow TiO_2 photocatalyst. Sci China Mater, 2016, 59: 1017–1026
35 Jin J, Huang SZ, Liu J, *et al.* Phases hybriding and hierarchical structuring of mesoporous TiO_2 nanowire bundles for high-rate and high-capacity lithium batteries. Adv Sci, 2015, 2: 1500070
36 Lin C, Fan X, Xin Y, *et al.* Monodispersed mesoporous $Li_4Ti_5O_{12}$ submicrospheres as anode materials for lithium-ion batteries: morphology and electrochemical performances. Nanoscale, 2014, 6: 6651–6660
37 Shin JY, Samuelis D, Maier J. Sustained lithium-storage performance of hierarchical, nanoporous anatase TiO_2 at high rates: emphasis on interfacial storage phenomena. Adv Funct Mater, 2011, 21: 3464–3472
38 Ali Z, Cha SN, Sohn JI, *et al.* Design and evaluation of novel Zn doped mesoporous TiO_2 based anode material for advanced lithium ion batteries. J Mater Chem, 2012, 22: 17625–17629
39 Hao R, Jiang B, Li M, *et al.* Fabrication of mixed-crystalline-phase spindle-like TiO_2 for enhanced photocatalytic hydrogen production. Sci China Mater, 2015, 58: 363–369
40 Liu Y, Lan K, Li S, *et al.* Constructing three-dimensional mesoporous bouquet-posy-like TiO_2 superstructures with radially oriented mesochannels and single-crystal walls. J Am Chem Soc, 2017, 139: 517–526
41 Han T, Chen Y, Tian G, *et al.* Hydrogenated TiO_2/$SrTiO_3$ porous microspheres with tunable band structure for solar-light photocatalytic H_2 and O_2 evolution. Sci China Mater, 2016, 59: 1003–1016

Acknowledgments This work was supported by the National High Technology Research and Development Program of China (2013AA050901), the National Basic Research Program of China (2015CB251100), the Thousand Youth Talents Program, the National Natural Science Foundation of China (51602173, 51371015 and 11674023), and China Postdoctoral Science Foundation (2016M591186). We thank Prof. Jiaping Wang, Fei Zhao, and Yufeng Luo for their help with the N_2 adsorption/desorption measurements.

Author contributions Zhu K, Shan Z, and Liu K proposed and designed the project. Zhu K performed the experiments and wrote the paper. Liu K, Sun Y, and Wang R revised and polished the paper. All the authors contributed to the general discussion.

Conflict of interest The authors declare that they have no conflicts of interest.

Supplementary information Experimental details, N_2 adsorption/desorption results, SEM images, XRD patterns, Raman spectra, EELS spectra, EDS spectra, the change curves for the diameter of the intermediate TiO_2 samples, TEM images, schematic diagrams, Li-ion battery performance measurements, and references are available in the online version of the paper.

Kunlei Zhu obtained his PhD degree at Tianjin University in 2015, and is now a postdoctoral research fellow at Tsinghua University. His research interests are focused on the syntheses of mesoporous materials and 2D materials for energy storage.

Zhongqiang Shan was born in 1957. He is a full professor at Tianjin University. His current research interests are focused on the energy storgae devices including Li-ion battries, Li-S batteries and supercapacitors.

Kai Liu obtained his PhD degree at Tsinghua University in 2008. He joined Tsinghua University as an associtate professor in 2015 after a period of postdoctoral research at Lawrence-Berkeley National Lab. His current research focuses on the mechanical and electrical properties of low-dimensinal materials and their applications.

快速制备均匀的高振实密度亚微米级二氧化钛介孔球及其在锂离子二次电池中的应用

朱坤磊[1,2], 孙颖慧[3], 王荣明[3], 单忠强[1*], 刘锴[2*]

摘要 随着人们对电动汽车和可穿戴电子产品需求的增加, 开发具有高体积比容量的锂离子二次电池非常必要, 特别是制备高振实密度的电极材料尤为重要. TiO_2是一种具有应用前景的阳极材料, 然而它们的振实密度普遍较低(通常小于<1 g cm^{-3}). 本论文报道了一种均匀的亚微米级TiO_2介孔球, 其振实密度高达1.62 g cm^{-3}. 以其作为锂离子二次电池的阳极材料时, 在高达24 mg cm^{-2}的负载量的情况下, TiO_2介孔球的体积比容量比其他对比TiO_2材料的体积比容量高出2倍之多. 制备该TiO_2介孔球仅需6 h的反应时间且产率接近100%, 因此其工业化生产可能性很大. 此外, 该制备方法的普适性非常好 , 其他高振实密度介孔材料, 如亚微米级$Li_4Ti_5O_{12}$介孔球, 也可采用类似方法制备. 因此, 本工作可为工业化制备高振实密度介孔材料及其在高体积比容量锂离子二次电池中的应用提供重要借鉴.